THE UNIVERSITY *of* EDINBURGH

Edinburgh Research Explorer

A low temperature X-ray single-crystal diffraction and polarised infra-red study of epidote

OPEN ACCESS

A low temperature X-ray single-crystal diffraction and polarised infra-red study of epidote

G. Diego Gatta[1,2], Matteo Alvaro[3], Geoffrey Bromiley[4]

[1]Dipartimento di Scienze della Terra, Università degli Studi di Milano, Via Botticelli 23,
 I-20133 Milano Italy
[2]CNR-Istituto per la Dinamica dei Processi Ambientali, Milano, Italy
[3]Crystallography Laboratory, Department of Geosciences, Virginia Tech, Blacksburg, Virginia 24060, U.S.A.
[4]School of GeoSciences and CSEC, The University of Edinburgh , UK

Corresponding Author:

G. Diego Gatta
Dip. Scienze della Terra
Universita' degli Studi di Milano
Via Botticelli, 23
I-20133 Milano, Italy
Tel. +39 02 503 15607
Fax +39 02 503 15597
E-Mail: diego.gatta@unimi.it

Abstract

The effects of low-temperature on the crystal structure of a natural epidote [$Ca_{1.925}$ $Fe_{0.745}Al_{2.265}Ti_{0.004}Si_{3.037}O_{12}(OH)$, a=8.8924(7), b=5.6214(3), c=10.1547(6)Å and β= 115.396(8)° at room conditions, Sp. Gr. $P2_1/m$] have been investigated with a series of structure refinements down to 100 K on the basis of X-ray single-crystal diffraction data. The reflection conditions confirm that the space group is maintained within the T-range investigated. Structural refinements at all temperatures show the presence of Fe^{3+} at the octahedral M(3) site only [%Fe(M3)=70.6(4)% at 295 K]. Only one independent proton site was located and two possible H-bonds occur, with O(10) as donor and O(4) and O(2) as acceptors. The H-bonding scheme is maintained down to 100 K and is supported by single crystal room-T Polarised FTIR data. FTIR Spectra over the region 4,000-2,500 cm^{-1} are dominated by the presence of a strongly pleochroic absorption feature which can be assigned to protonation of O(10)-O(4). Previously unobserved splitting of this absorption features is consistent with a NNN influence due to the presence of Al and Fe^{3+} on the nearby M3 site. An additional relatively minor absorption feature in FTIR spectra can be tentatively assigned to protonation of O(10)-O(2). Low-T does not affect significantly the tetrahedral and octahedral bond distances and angles, even when distances are corrected for "rigid body motions". A more significant effect is observed for the bond distances of the distorted Ca(1)- and Ca(2)-polyhedra, especially when corrected for "non-correlated motion". The main low-T effect is observed on the vibrational regime of the atomic sites, and in particular for the two Ca-sites. A significant reduction of the magnitude of the thermal displacement ellipsoids, with a variation of U_{eq} (defined as one third of the trace of the orthogonalised U_{ij} tensor) by ~40% is observed for the Ca-sites between 295 and 100 K. Within the same T-range, the U_{eq} of the octahedral and oxygen sites decrease similarly by ~35%, whereas those of the tetrahedral cations by ~22%.

Keywords: epidote, low-temperature, X-ray single-crystal diffraction, polarised single crystal FTIR, structurally incorporated water, hydrogen bonding.

Introduction

Epidotes are a class of hydrous sorosilicates with the following general formula: $A(1)A(2)M(1)M(2)M(3)(Si_2O_7)(SiO_4)O(OH)$, where the A(1) and A(2) sites are mainly occupied by Ca (with coordination number CN>6), and M(1), M(2) and M(3) sites are mainly occupied by Al and Fe^{3+} (with CN=6). In nature cationic substitution can occur at the A(1) and A(2) and at the M(1) and M(3) sites (Franz and Liebscher 2004). The term "epidote" *sensu stricto* (s.s.) should be used for members with composition $Ca_2Al_2Fe^{3+}Si_3O_{12}(OH)$, according to the Commission of the International Mineralogical Association. Epidotes s.s. occur in several geological environments. They usually form during low grade metamorphism and hydrothermal activity (250–400°C, 0.1-0.2 GPa), and can be stable over a wide range of pressures and temperatures in continental and oceanic crust (Poli and Schmidt 1998, 2004). Epidote s.s. is common in metamorphosed basalts and gabbros, but also in schists and marbles where its crystals are frequently found infilling vugs or veins. Less common magmatic epidote has been also found (Schmidt and Poli 2004). Several studies have shown how the stability of epidotes s.s. is controlled by *P*, *T*, by the Al/Fe^{3+} ratio, oxygen fugacity and fluid composition (Holdaway 1972, Liou 1973, Bird and Helgeson 1980, Bird et al. 1988, Klemd 2004).

The crystal structure of epidote s.s. is monoclinic, with space group $P2_1/m$. Several studies showed how the unit-cell constants are significantly correlated to the amount of Fe^{3+}, coupled to a possible symmetry reduction (to *Pm, P2$_1$ or P$\bar{1}$*) due to cation ordering (Franz and Liebscher 2004 and references therein). The crystal structure of epidote is complex and consists of both single silicate tetrahedra, SiO_4, and double silicate tetrahedra, Si_2O_7, and continuous chains of AlO_6 and $AlO_4(OH)_2$ octahedra (running parallel to the *b*-axis and where Fe^{3+} can replace Al), that are bridged by single SiO_4 and double Si_2O_7 tetrahedral groups (Fig. 1). The octahedral chains are arranged in parallel planes, resulting in perfect {001} cleavage planes. The formula of epidote s.s. can be expressed as: $^{A1}Ca^{A2}Ca^{M1}(Al,Fe^{3+})^{M2}(Al)^{M3}(Al,Fe^{3+})O(SiO_4)(Si_2O_7)(OH)$; therefore epidote s.s. represents a solid solution between $Ca_2Al_3Si_3O_{12}(OH)$ and $Ca_2Fe^{3+}Al_2Si_3O_{12}(OH)$, as the replacement of Al by Fe^{3+} does not significantly exceed one atom per formula unit (a.p.f.u.). A series of experiments proved the preference of Fe^{3+} for M(3) and M(1) sites at ambient and non-ambient conditions (among those: Dollase 1968, 1969, 1971,

1973; Gabe et al. 1973; Langer and Raith 1974; Nozik et al. 1978; Bird and Helgeson 1980; Carbonin and Molin 1980; Stergiou et al. 1987; Bird et al. 1988; Catti et al. 1988; Kvick et al. 1988; Bonazzi and Menchetti 1995, 2004; Comodi and Zanazzi 1997; Giuli et al. 1999; Gatta et al. 2011).

The thermo-elastic behaviour of an epidote from Valmalenco, with $Fe_{0.745}$ a.p.f.u., was recently investigated at high-P and high-T by means of synchrotron X-ray powder diffraction (Gatta et al. 2011) and at high-T by neutron single-crystal diffraction (on the basis of two structure refinements at 295 and 1,070 K; Gatta et al. 2010). The nuclear structure of epidote refined on the basis of the neutron diffraction data allowed description of: *a*) the T-induced structural evolution and mean deformation mechanisms; *b*) the absence of T-induced disordering phenomena (within temperature and time of the experiment), and *c*) the variation of the thermal displacement regime of all the atomic sites, including the H-site. In order to provide a full description of the thermo-elastic behaviour of epidote, the aim of this study is the description of the low-T behaviour the sample previously investigated by Gatta et al. (2010, 2011) through a series of X-ray single-crystal structure refinements between 295 and 100 K. This will allows a description of the main deformation mechanisms (e.g. polyhedral tilting, potential changes in H-bonding with cooling) along with changes of the atomic libration regime. Only one experiment was previously performed on epidote $[(Ca_{1.98}Mn_{0.02})(Fe_{0.81}Al_{2.19})Si_3O_{12}(OH)]$ at low-T, on the basis of one neutron structure refinement at 15 K (Kvick et al. 1988). In addition, examination of OH stretching modes and their pleochroic scheme is performed on the basis of single-crystal polarized infrared (FTIR) spectroscopy at room-T.

Experimental methods

A dark-green single-crystal of epidote s.s. (MA6, crystal size: 140 x 90 x 50 μm) from the same sample used by Gatta et al. (2010, 2011) was used in this study. This epidote was collected from the intrusive/metamorphic complex of Val Sissone, Valmalenco (Rhetic Alps, Italy). The sample and the chemical analysis $[Ca_{1.925}Fe_{0.745}Al_{2.265}Ti_{0.004}Si_{3.037}O_{12}(OH)$, in Bedognè et al. 1993] have been kindly provided by Museo di Storia Naturale, Milano, Italy. Under a polarised microscope, the crystal appeared free of defects, twinning or zoning.

Diffraction data from the MA6 crystal were collected at 295 (room-T), 270, 245, 220, 195, 170, 145, 120 and 100 K with decreasing temperature (Table 1a), and at 110, 135, 160, 185, 210, 285 and 295 K with increasing temperature (Table 1b). Intensity data were collected at the Crystallography Lab, Virginia Tech, using a Gemini diffractometer (Oxford Diffraction – Varian inc.) equipped with an EOS-CCD type detector and with a monochromatic (graphite) beam from a MoKα-radiation source (Enhance X-ray optics) operating at 50 kV and 40 mA. Detector-crystal distance was fixed at 50 mm. A series of ω scans were used to collect a complete hemisphere of data to a resolution of 0.6 Å, with a fixed exposure time of 10 s per 1° frame reaching a completeness of 99.5%. For the low-T data collections, the crystal was slowly cooled by using a Cryojet open-flow nitrogen gas system (temperature stability better than ±0.1 K and absolute temperature uncertainty at the crystal position less than ±2 K). The diffraction patterns at all temperatures confirm a metrically monoclinic lattice with reflection conditions consistent with space group $P2_1/m$. Lorentz-polarization and analytical absorption corrections by Gaussian integration based upon the physical description of the crystal (CrysAlis, Oxford Diffraction 2010) were performed. Further details pertaining to the data collections are provided in Tables 1a and 1b.

Doubly-polished sections of the epidote sample were prepared from a high quality euhedral single crystal for examination of OH stretching modes using FTIR spectroscopy at the Dept. of Earth Sciences, University of Cambridge, UK. Sections parallel to (001) and (010) were mounted onto glass slides using Crystalbond™ and polished to a thickness of less than 10 μm. Prior to IR examination sections were soaked for 24 hours in analytical-grade acetone to remove them from glass slides. Polarized MIR spectra were obtained using a Bruker IFS113V spectrometer with a Bruker IRscopeII IR microscope using a Globar MIR source, KBr beamsplitter, MCT detector and a wire strip polarizer. Samples were placed over pinhole apertures for IR measurements and crystallographic axes aligned with respect to the reference frame of the IR microscope. The optics of the microscope were continuously purged with purified air to minimize unwanted absorption due to H_2O and CO_2. A total of 512 scans were obtained for each measurement using a resolution of 2 cm^{-1}.

Results: Structure refinements

The intensity data of epidote collected at room temperature were processed with the programs E-STATISTICS and ASSIGN-SPACEGROUP, implemented in the WinGX suite (Farrugia 1999). The statistics of distributions of the normalized structure factors (E's) and the Sheldrick's $\lvert E^2\text{-}1 \rvert$ criterion showed that the structure is centrosymmetric (at 82.6% likelihood, $\lvert E^2\text{-}1 \rvert = 0.927$), suggesting the space group $P2_1/m$ as highly likely. The anisotropic structure refinement was then performed in the space group $P2_1/m$ using the SHELX-97 software (Sheldrick 1997), starting from the atomic coordinates of Gatta et al. (2010). Only the H site was modeled as isotropic. Neutral atomic scattering factors for Ca, Al, Fe, Si, O and H were taken from the *International Tables for X-Ray Crystallography* (Wilson and Price 1999). The secondary isotropic extinction effect was corrected according to Larson's formalism, as implemented in the SHELXL-97 package. In the first cycles of the refinement, a mixed Al/Fe scattering curve was used for the octahedral M(1) and M(3) sites. However, a significant amount of Fe was only found at the M(3) site, consistent with the experimental finding of Gatta et al. (2010). Convergence was rapidly achieved after a few cycles of refinement. All the principal mean-square atomic displacement parameters were positively defined and the variance-covariance matrix showed no significant correlation among the refined parameters. No peak larger than +0.8/-0.7 fm/Å^3 was present in the final difference-Fourier map of the electron density (Table 1a). The final agreement index (R_1) was 0.0357 for 120 refined parameters and 1465 unique reflections with $Fo>4\sigma(Fo)$ (Table 1a). Atomic coordinates are reported in Table 2a, displacement parameters in Tables 3a and 4a (deposited). Relevant bond lengths and angles are listed in Tables 5.

The intensity data collected at low-T were processed following the same protocol used for the refinement at 295 K. At all temperatures reflection conditions and statistic criteria suggested that epidote maintains its symmetry. The anisotropic structural refinements were performed starting from the structural model previously refined at 295 K. The quality of all the low-T structure refinements is high (Tables 1a and 1b), with no significant residuals in the difference-Fourier map of the electron density and no significant correlation among the refined parameters. The refined site positions at 100 K are reported in Table 2b, and displacement parameters in Table 3b

and 4b. Bond lengths and angles are listed in Table 5. Site positions together with their thermal parameters, relevant bond lengths and angles and other geometrical parameters pertaining to the other low-T refinements are given in Table 6 (deposited).

At all temperatures refinements imply an unrealistically short O(10)-H(1) bond distance (*i.e.* ~0.7-0.8 Å), as usually expected for X-ray diffraction data when proton coordinates are refined. In order to obtain a more realistic configuration of the hydroxyl group the atomic position of the H-site was deduced on the basis of the maxima of the difference-Fourier map of the electron density, and not refined. This protocol led to more realistic bond distance values (O-H > 0.9 Å, Tables 5 and 6), giving a more reliable picture of the H-bonding scheme.
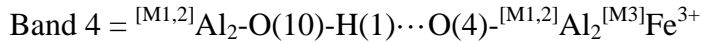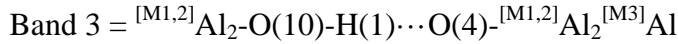
Results: Infrared spectra

Polarised single crystal FT-Infrared (FT-IR) absorbtion spectra obtained from epidote are consistent with incorporation of protons as OH groups with no evidence for the presence of molecular water. Spectra from the sample epidote MA6, between 3,800 and 3,000 cm^{-1}, are shown in Fig. 2. Spectra were obtained using incident radiation polarised parallel to the principle crystallographic axes to aid band assignment and spectra were thickness and background corrected using a linear background over the wavenumber range 4,000-2,800 cm^{-1} and were fitted using the 'Find Peaks' routine in IGOR using Lorentzian peak profiles (method outlined in Bromiley et al. 2010). Results of spectral fitting are shown in Table 7. E//[010] and E/[001] spectra could be fitted with 4 peaks. For E//[100] there is minimal absorption over the range 4,000-2,800 cm^{-1} and a higher signal to noise ratio in the spectrum; hence band deconvolution for this spectrum is inherently much less accurate. A best fit for this spectrum is obtained using 3 Lorentzian peaks. Comparison of all fitting data suggest a minimum of 5 distinct absorption bands in the IR spectra from epidote over the range of stretching frequencies due to O-H vibration: band 1 (3,470 cm^{-1} corresponding to peaks A3, B4 and C4) with the pleochroic scheme [001]>>[100]≥[010], band 2 (3,400 cm^{-1} corresponding to peaks B3) co-linear with [010], band 3 (3,385 cm^{-1} corresponding to peak C3) which is almost co-linear with [001], band 4 (3,352 cm^{-1} corresponding to peaks B2 and C2) with [001]>>[010], and band 5 (3,257 cm^{-1} corresponding to bands A1, B1 and C1) with [001]>>[100]>[010]. Additionally, peak A2 could represent a doublet consisting of bands 3 and 4, although

intensities are too low meaningfully assign this feature to less than 1 peak. Based on results the following order of decreasing OH band total absorption, positively correlated to the concentration of H giving rise to each band, can be identified: band 3>band 4>band 5>band 1>band 2.

Discussion and conclusions

At room-T, the X-ray structure refinement leads to atomic positions in good agreement with the experimental findings of Gatta et al. (2010). Our refinement confirms the presence of Fe^{3+} at the M(3) site only [%Fe(M3)= 70.6(4)%] (Table 2a), in accordance with previous characterisation of the same epidote sample. This result agrees also with observations made by Bonazzi and Menchetti (1995), who reported that Fe^{3+} is found at the M(1) site only when the volume of the M(3) polyhedron is higher than 11 $Å^3$. Our structure refinement leads to a refined volume of the M(3) polyhedron of 10.85 $Å^3$ (Table 5). Only one independent proton site was located, according to Kvick et al. (1988) and Gatta et al. (2010). Two possible hydrogen bonds occur, with O(10) as *donor* and O(2) and O(4) as *acceptors*. The configuration of the H-bond with O(4) appears energetically less costly [with H(1)···O(4) = 2.016(2) Å, O(10)···O(4) = 2.937(3) Å and O(10)–H(1)···O(4) = 173.9(10)°] than that with O(2) as acceptor [with H(1)···O(2) = 2.472(2) Å, O(10)···O(2)= 2.823(3) Å and O(10)–H(1)···O(2) = 102.0(10)°]. Previously acquired IR spectra from epidote consist of a single O-H stretching absorption band vibrating between 3,330 and 3,380 cm^{-1}, or splitting of this OH band only in Mn^{3+}-bearing samples (Liebscher 2004). Della Ventura et al. (1996) ascribed splitting of the OH band due to the Jahn-Teller effect that Mn^{3+} exerts on the M3 cation, where substitution of Mn for Al flattens the M(3) octahedron along the O(4)-O(8) direction and shortens the M(3)-O(4) bond length compared to the Al-Fe^{3+} solid solution series (with an increase the H(1)···O(4) distance and shift the OH band to higher wavenumbers). Aside from this splitting, a continuous shift in OH stretching frequency in epidote spectra is noted in Al-Fe^{3+} solid solutions as a function of Fe content (Liebscher 2004). Spectra obtained from our epidote have a similar pleochroic scheme to that noted by Hanisch and Zemann (1966), with maximum absorption parallel to [001] and relatively minor absorption parallel to [010] and [100]. However, here we note that absorption parallel to [010] is

slightly greater than [100], in contrast to the experimental findings of Hanisch and Zemann (1966). In our spectra we also observe clear splitting of the OH band into at least 5 resolvable components (Fig. 2, Table 7). Most absorption is due to a prominent doublet; deconvolution of the spectra demonstrate that this feature consists of OH bands at 3,352 cm^{-1} (band 3) and 3,386 cm^{-1} (band 4). The average of these 2 bands is, within *esd's*, the same as the predicted OH band frequency for epidote based on published data of the effect of Fe content on OH stretching frequency, as noted by Liebscher (2004). It appears likely that splitting of the main OH band is a common feature in epidote and zoisite IR spectra, but simply one which has not been previously resolvable. It should be noted that these 2 prominent bands (*i.e.* 3 and 4) have slightly different polarisations, consistent with splitting due to some NNN interaction (*i.e.* NNN interactions result in a slight change in O-H orientation). On the basis of X-ray (this study) and neutron (Gatta et al. 2010) structure refinements at room-*T*, we suggest that the splitting of the main OH absorption band is due to Al-Fe^{3+} solid solution. We can then assign splitting of OH bands to Fe/Al occupation of adjacent M(3) sites (NNN):

Band 3 = [M1,2]Al$_2$-O(10)-H(1)$\cdots$O(4)-[M1,2]Al$_2$[M3]Al

Band 4 = [M1,2]Al$_2$-O(10)-H(1)$\cdots$O(4)-[M1,2]Al$_2$[M3]Fe^{3+}

considering the slightly different Al-O and Fe^{3+}-O bond distances. We might tentatively assign band 2 to a second H bridge, *i.e.* O(10)–H(1)$\cdots$O(2) on the basis of band polarisation and stretching frequency. Based on calibration of O$\cdots$O distances with O-H stretching frequency, we would predict that band 2 is due to protonation of an O-O edge approximately 2.8 Å, in agreement to the structure refinement [with O(10)$\cdots$O(2) = 2.822(2)Å, neutron data at 295 K by Gatta et al. 2010, O(10)$\cdots$O(2) = 2.823(3) Å, X-ray data at 295 K, this study]. Other bands (1 and 5, Fig. 2, Table 7) can be assigned to O-H vibration coupled with lattice vibration modes.

The diffraction data collected at low-*T* show that, within the precision and accuracy of our CCD data, unit-cell constants vary between 295 and 100 K following the trends reported for the same epidote sample by Gatta et al. (2011), by means of synchrotron X-ray powder diffraction up to 1,169 K (Fig. 4). The high-*T* diffraction experiment led to the following thermo-elastic equations:

$V(T)/V_0 = 1 + s_1 \cdot T + s_2 \cdot T^2 = 1 + 2.1(1) \cdot 10^{-5} \cdot T + 7.3(9) \cdot 10^{-9} \cdot T^2$, where s_1 and s_2 are refinable parameters;

$a(T)/a_0 = 1 + 4.9(5) \cdot 10^{-6} \cdot T + 1.7(3) \cdot 10^{-9} \cdot T^2$;

$b(T)/b_0 = 1 + 8.7(5)\cdot10^{-6}\cdot T + 2.4(3)\cdot10^{-9}\cdot T^2;$

$c(T)/c_0 = 1 + 9.5(5)\cdot10^{-6}\cdot T + 2.9(3)\cdot10^{-9}\cdot T^2.$

A slight decrease of the monoclinic angle at low-T is observed, in agreement with the previous high-T experiment (Gatta et al. 2011). The low-T structure refinements show little or no significant variation in the geometrical parameters (*e.g.* atomic positions, intra- and inter-polyhedral distance and angles, polyhedral volumes). The tetrahedral and octahedral bond distances do not vary significantly over the T-range investigated, even when bond distances are corrected for "rigid body motions" following Downs et al. (1992) and Downs (2000). Structure refinements at all T confirm the presence of Fe^{3+} at the M(3) site only, along with Al^{3+} [*e.g.* %Fe(M3)$_{100K}$ = 69.6(4)%] (Table 2b).

The main low-T effect is observed on the vibrational regime of the atomic sites (Fig. 5), in particular for the two Ca-sites (*i.e.* Ca(1) and Ca(2)). A significant monotonic reduction of the magnitude of the thermal displacement ellipsoids, with a variation of U_{eq} (defined as one third of the trace of the orthogonalised U_{ij} tensor; the anisotropic displacement factor exponent takes the form: $-2\pi^2[(ha^*)^2U_{11} +(kb^*)^2U_{22}...+ 2hka^*b^*U_{12}]$) by ~40% is observed for both the Ca-sites between 295 and 100 K (Fig. 6, Table 2a, 2b and 6). Evolution of the root-mean-square components of the thermal ellipsoids (R1, R2 and R3, where R1 and R3 represent the longest and the shortest components, respectively, Tables 4a and 4b) is shown in Fig. 6. Whereas for the Ca(2) site a similar monotonic reduction of the three components occur, for the Ca(1) site the R1 and R2 apparently converge to similar values at $T\leq150$ K. The vibrational regime of the Ca(1) and Ca(2) sites is slightly different over the T-range investigated: the Ca(1) site shows a lower U_{eq} and a less pronounced anisotropy (represented by R1/R3, Tables 4a and 4b) than Ca(2) at any temperature. This is basically due to the different coordination shell of the two cationic sites, with longer bond distances for Ca(2) (Tables 5 and 6). The effect of the anisotropic vibrational regime of Ca(1) and Ca(2) on the Ca-O bond distance has been considered through the correction of the distances for "non-correlated motion" following the protocol of Busing and Levy (1964). At room-T, the corrected Ca-O distances appear to be longer than un-corrected ones within 0.008-0.013 Å, whereas at 100 K the difference decreases within 0.004-0.007 Å (Table 5).

Between 295 and 100 K, the U_{eq} of the octahedral and oxygen sites decreases similarly by ~35%, whereas those of the tetrahedral cations decrease by ~22%. As already observed by Gatta et al. (2010) and Kvick et al. (1988), thermal displacement ellipsoids of the oxygen sites are only slightly pronounced (Tables 3a, 3b and 6). The most significant anisotropy is observed for the O(3), O(8) and O(9) oxygen sites, but still modest (with R1/R3<3). This effect, which is maintained even at low-T (Tables 3a, 3b and 6), and might be driven by rotation of the Si(2)-tetrahedron due to the presence of Fe^{3+} at the M(3) site, if compared to a Fe-free structure (*i.e.* zoisite, Smith et al. 1987).

References

Bedognè F., Montrasio A., Sciesa E. (1993) Valmalenco – I minerali della provincia di Sondrio. Bettini, Sondrio (Italy), 275 p.

Bird, D.K. and Helgeson, H.C. (1980) Chemical interaction of aqueous solutions with epidote-feldspar mineral assemblages in geologic systems, I: thermodynamic analysis of phase relations in the system $CaO-FeO-Fe_2O_3-Al_2O_3-SiO_2-H_2O-CO_2$. Am J Science 280:907–941.

Bird, D.K., Cho, M., Janik, C.J., Liou, J.G., and Caruso, L.J. (1988) Compositional, order-disorder, and stable isotopic characteristics of Al-Fe epidote, state 2–14 drill hole, Salton Sea geothermal system. J Geophys Res 93(B11):13135-13144.

Bonazzi P, Menchetti S (1995) Monoclinic members of the epidote group: Effect of the $Al \leftrightarrow Fe^{3+} \leftrightarrow Fe^{2+}$ substitution and of the entry of REE^{3+}. Mineral Petrol 53:133-153.

Bonazzi P, Menchetti S (2004) Manganese in monoclinic members of the epidote group: piemontite and related minerals. In G. Franz and A. Liebscher, Eds., Epidotes, Vol. 56, p. 495-552. Reviews in Mineralogy and Geochemistry, Mineralogical Society of America and Geochemical Society, Washington, U.S.A.

Busing WR, Levy HA (1964) The effect of thermal motion on the estimation of bond lengths from diffraction measurements. Acta Cryst 17:142-146.

Bromiley G.D., Nestola F., Redfern S.A.T., Zhang M. (2010). Water incorporation in synthetic and natural $MgAl_2O_4$ spinel. Geochim. Cosmochi. Acta 74:705-718.

Carbonin S, Molin G (1980) Crystal-chemical considerations of eight metamorphic epidotes. N Jb Mineral Abh 139:205-215.

Catti M, Ferraris G, Ivaldi G (1988) Thermal behaviour of the crystal structure of strontian piemontite. Am Mineral 73:1370-1376.

Comodi P, Zanazzi PF (1997) The pressure behaviour of clinozoisite and zoisite. An X-ray diffraction study. Am Mineral 82:61-68.

Della Ventura G, Mottana A, Parodi GC, and Griffin WL (1996) FTIR spectroscopy in the OH-stretching region of monoclinic epidotes from praborna (St. Marcel, Aosta valley, Italy). Eur J Mineral 8:655-665.

Dollase WA (1968) Refinement and comparison of the structures of zoisite and clinozoisite. Am Mineral 53:1882-1898.

Dollase WA (1969) Crystal structure and cation ordering of piemontite. Am Mineral 54:710-17.

Dollase WA (1971) Refinement of the crystal structure of epidote, allanite and hancockite. Am Mineral 56:447-464.

Dollase WA (1973) Mössbauer spectra and iron distribution in the epidote-group minerals. Z Kristallogr 138:41–63.

Downs RT (2000) Analysis of harmonic displacement factors. In R.M. Hazen and R.T. Downs, Eds., High-Temperature and High-Pressure Crystal Chemistry, Vol. 41, p. 61-117. Reviews in Mineralogy and Geochemistry, Mineralogical Society of America and Geochemical Society, Washington, U.S.A.

Downs RT, Gibbs GV, Bartelmehs KL, Boisen Jr.MB (1992) Variations of bond lengths and volumes of silicate tetrahedra with temperature. Am Mineral 77:751-757.

Farrugia LJ (1999) WinGX suite for small-molecule single-crystal crystallography. J Appl Crystallogr 32:837-838.

Franz G, Liebscher A (2004) Physical and chemical properties of epidote minerals – An Introduction. In G. Franz and A. Liebscher, Eds., Epidotes, Vol. 56, p. 1-81. Reviews in Mineralogy and Geochemistry, Mineralogical Society of America and Geochemical Society, Washington, U.S.A.

Gabe EJ, Portheine FC, Whitlow SH (1973) A reinvestigation of the epidote structure: confirmation of the iron location. Am Mineral 58:218-223.

Gatta GD, Meven M, and Bromiley G (2010) Effects of temperature on the crystal structure of epidote: A neutron single-crystal diffraction study at 293 and 1,070 K. Phys Chem Minerals 37(7):475-485.

Gatta GD, Merlini M, Lee Y, and Poli S (2011) Behavior of epidote at high pressure and high temperature: A powder diffraction study up to 10 GPa and 1,200 K. Phys Chem Mineral 38(6):419-428.

Giuli G, Bonazzi P, Menchetti S (1999) Al-Fe disorder in synthetic epidotes: a single-crystal X-ray diffraction study. Am Mineral 84:933-936.

Hanisch K, Zemann J (1966) Messung des Ultrarot-Pleochroismus von Mineralen. IV.

Der Pleochroismus der OH-Streckfrequenz in Epidot. N Jb Mineral Mon 1966:19-23.

Holdaway MJ (1972) Thermal stability of Al-Fe epidotes as a function of fO$_2$ and Fe content. Contrib Min Petrol 37:307–340.

Klemd R (2004) Fluid inclusions in epidote minerals and fluid development in epidote-bearing rocks. In G. Franz and A. Liebscher, Eds., Epidotes, Vol. 56, p. 197-234. Reviews in Mineralogy and Geochemistry, Mineralogical Society of America and Geochemical Society, Washington, U.S.A.

Kvick Å, Pluth JJ, Richardson Jr. JW, Smith JV (1988) The ferric ion distribution and hydrogen bonding in epidote: a neutron diffraction study at 15 K. Acta Cryst B44:351-355.

Langer K, Raith M (1974) Infrared spectra of Al-Fe(III)-epidotes and zoisites Ca$_2$(Al$_{1-p}$Fe$^{3+}_p$)Al$_2$O(OH)[Si$_2$O$_7$][SiO$_4$]. Am Mineral 59:1249-1258.

Liebscher A (2004) Spectroscopy of epidote minerals. In G. Franz and A. Liebscher, Eds., Epidotes, Vol. 56, p. 125-170. Reviews in Mineralogy and Geochemistry, Mineralogical Society of America and Geochemical Society, Washington, U.S.A.

Liebscher A, Gottschalk M, Franz G (2002) The substitution Fe^{3+}-Al and the isosymmetric displacive phase stransition in synthetic zoisite: A powder X-ray and infrared spectroscopy study. Am Mineral 87:909-921.

Liou JG (1973) Synthesis and stability relations of epidote, Ca$_2$Al$_2$FeSi$_3$O$_{12}$(OH). J Petrol 14:381–413.

Nozik YK, Kanepit VN, Fykin LY, Makarov YS (1978) A neutron diffraction study of the structure of epidote. Geochem Int 15:66-69.

Oxford Diffraction (2010) Oxford Diffraction Ltd., Xcalibur CCD system, CrysAlis Software system.

Poli S, and Schmidt MW. (1998) The high-pressure stability of zoisite and phase relationships of zoisite-bearing assemblages. Contrib Mineral Petrol 130:162-175.

Poli S, Schmidt MW (2004) Experimental subsolidus studies on epidote minerals. In G. Franz and A. Liebscher, Eds., Epidotes, Vol. 56, p. 171-195. Reviews in Mineralogy and Geochemistry, Mineralogical Society of America and Geochemical Society, Washington, U.S.A.

Robinson K, Gibbs GV, Ribbe PH (1971) Quadratic Elongation: A Quantitative

Measure of Distortion in Coordination Polyhedra. Science 172:567-570.

Sheldrick GM (1997) SHELX-97. Programs for crystal structure determination and refinement. University of Göttingen, Germany.

Schmidt MW, Poli S (2004) Magmatic epidotes. In G. Franz and A. Liebscher, Eds., Epidotes, Vol. 56, p. 399-430. Reviews in Mineralogy and Geochemistry, Mineralogical Society of America and Geochemical Society, Washington, U.S.A.

Smith JV, Pluth JJ, Richardson Jr. JW, Kvick Å (1987) Neutron diffraction study of zoisite at 15 K and X-ray study at room temperature. Z Kristallogr 179:305-321.

Stergiou AC, Rentzeperis PJ, Sklavounos S (1987) Refinement of the crystal structure of a medium iron epidote. Z. Kristallogr 178:297-305.

Wilson, A.J.C. and Price, E., Eds. (1999) International Tables for Crystallography Volume C, Kluwer Academic Publishers, Dordrecht, The Netherlands.

Table 1a. Details pertaining to the data collection and refinement of epidote at different temperatures decreasing temperature.

T (K)	295	270	245	220	195	170	145	120	100
a (Å)	8.8924(7)	8.8942(7)	8.8841(6)	8.8793(7)	8.8809(7)	8.8871(6)	8.8803(11)	8.8906(14)	8.8912(9)
b (Å)	5.6214(3)	5.6243(3)	5.6214(2)	5.6161(3)	5.6197(3)	5.6278(3)	5.6218(6)	5.6423(7)	5.6312(4)
c (Å)	10.1547(6)	10.1571(7)	10.1387(6)	10.1499(7)	10.1537(7)	10.1498(6)	10.1481(11)	10.1516(14)	10.1494(8)
β(°)	115.396(9)	115.384(9)	115.378(6)	115.377(9)	115.365(9)	115.332(7)	115.415(15)	115.297(18)	115.311(11)
V (Å^3)	458.56(5)	459.04(5)	457.47(4)	457.30(5)	457.90(6)	458.83(4)	457.59(9)	460.41(11)	459.38(7)
Space group	$P2_1/m$	$P2_1/m$	$P2_1/m$	$P2_1/m$	$P2_1/m$	$P2_1/m$	$P2_1/m$	$P2_1/m$	$P2_1/m$
Z	2	2	2	2	2	2	2	2	2
θ range (°)	4.58-37.39	4.58-37.38	4.59-37.57	4.59-37.53	4.59-37.44	4.59-37.49	4.59-37.56	4.59-37.57	4.59-37.49
No. of refl. with $Fo > 4\sigma(Fo)$	1465	1491	1508	1490	1481	1489	1427	1463	1461
No. all refl.	2488	2477	2486	2479	2481	2482	2480	2480	2481
R_{int}	0.0588	0.0602	0.0594	0.0599	0.0636	0.0612	0.0687	0.0692	0.0666
R_1	0.0357	0.0362	0.0357	0.0363	0.0365	0.035	0.0371	0.0385	0.0373
wR_2	0.0465	0.0465	0.0455	0.0484	0.0469	0.0468	0.0485	0.0496	0.0484
R_1 (all refl.)	0.0821	0.0772	0.079	0.0798	0.081	0.0795	0.0888	0.0867	0.086
wR_2 (all refl.)	0.051	0.0503	0.0501	0.0525	0.0515	0.0513	0.0552	0.055	0.0541
No. refined parameters	120	120	120	120	120	120	120	120	120
Residuals (e^-/ Å$_3$)	-0.72/+0.81	-0.96/+0.90	-0.97/+0.95	-0.84/+0.94	-0.84/+0.84	-0.78/+0.81	-1.02/+1.13	-0.85/+1.10	-0.93/+1.01

Note: $R_{int} = \Sigma \mid F_{obs}^2 - F_{obs}^2(mean) \mid / \Sigma [F_{obs}^2]$; $R_1 = \Sigma(\mid F_{obs} \mid - \mid F_{calc} \mid)/\Sigma \mid F_{obs} \mid$; $wR_2 = [\Sigma[w(F^2_{obs} - F^2_{calc})^2]/\Sigma[w(F^2_{obs})^2]]^{0.5}$, $w = 1/ [\sigma^2(F_{obs}^2) + (0.01*P)^2]$, $P = (Max (F_{obs}^2, 0) +2*F_{calc}^2)/3$.

Table 1b. Details pertaining to the data collection and refinement of epidote increasing temperature.

T (K)	295	285	210	185	160	135	110
a (Å)	8.9007(4)	8.8948(6)	8.8963(6)	8.8983(6)	8.8941(6)	8.8895(7)	8.8895(7)
b (Å)	5.6263(2)	5.6275(2)	5.6215(3)	5.6257(2)	5.6209(2)	5.6203(3)	5.6203(3)
c (Å)	10.1654(4)	10.1549(6)	10.1385(6)	10.1509(4)	10.1455(6)	10.1219(7)	10.1219(7)
β(°)	115.442(5)	115.430(7)	115.378(9)	115.371(6)	115.348(6)	115.357(9)	115.357(9)
V (Å^3)	459.69(3)	459.06(4)	458.11(5)	459.13(4)	458.37(4)	456.99(5)	456.99(5)
Space group	$P2_1/m$	$P2_1/m$	$P2_1/m$	$P2_1/m$	$P2_1/m$	$P2_1/m$	$P2_1/m$
Z	2	2	2	2	2	2	2
θ range (°)	4.43-37.45	4.43-37.47	4.44-37.48	4.44-37.42	4.45-37.52	4.46-37.54	4.46-37.54
No. of refl. with $Fo> 4\sigma(Fo)$	1517	1520	1542	1533	1529	1512	1522
No. all refl.	2506	2496	2498	2491	2491	2493	2481
R_{int}	0.0544	0.0569	0.0553	0.0578	0.057	0.061	0.0593
R_1	0.0343	0.0364	0.0357	0.0351	0.034	0.0361	0.0349
wR_2	0.0447	0.0473	0.0465	0.0463	0.0445	0.0463	0.0454
R_1 (all refl.)	0.0745	0.0803	0.0757	0.0728	0.0739	0.0748	0.0735
wR_2 (all refl.)	0.0485	0.0522	0.0507	0.05	0.0487	0.0502	0.0494
No. refined parameters	120	120	120	120	120	120	120
Residuals (e^-/ Å$_3$)	-0.76/+0.64	-0.77/+0.88	-0.77/+0.82	-0.69/+0.93	-0.75/+0.65	-0.79/+0.98	-0.88/+0.83

Note: $R_{int} = \Sigma \mid F_{obs}^2 - F_{obs}^2(\text{mean}) \mid / \Sigma [F_{obs}^2]$; $R_1 = \Sigma(|F_{obs}| - |F_{calc}|)/\Sigma|F_{obs}|$; $wR_2 = [\Sigma[w(F^2_{obs} - F^2_{calc})^2]/\Sigma[w(F^2_{obs})^2]]^{0.5}$, $w= 1/ [\sigma^2(F_{obs}^2) + (0.01*P)^2]$, $P = (\text{Max} (F_{obs}^2, 0) +2*F_{calc}^2)/3$.

Table 2a. Refined fractional atomic coordinates and equivalent isotropic temperature factors ($\mathring{A}^2$), with standard deviations in parentheses, based on the diffraction data collected at 295 K. U_{eq} is defined as one third of the trace of the orthogonalised U_{ij} tensor.

Site	x/a	y/b	z/c	U_{eq}
Ca(1)	0.75768(8)	0.75	0.15176(6)	0.01085(13)
Ca(2)	0.60521(8)	0.75	0.42409(7)	0.01360(14)
Si(1)	0.33944(10)	0.75	0.04753(8)	0.00677(16)
Si(2)	0.68373(11)	0.25	0.27475(9)	0.00721(16)
Si(3)	0.18402(10)	0.75	0.31841(8)	0.00674(16)
M(1)	0	0	0	0.00623(17)
M(2)	0	0	0.5	0.00679(17)
M(3)	0.29339(6)	0.25	0.22427(5)	0.00726(15)
O(1)	0.23390(16)	-0.0056(3)	0.04093(14)	0.0088(3)
O(2)	0.30378(18)	-0.0182(3)	0.35497(14)	0.0098(3)
O(3)	0.79491(18)	0.0137(3)	0.33974(15)	0.0110(3)
O(4)	0.0531(2)	0.25	0.1293(2)	0.0077(4)
O(5)	0.0413(2)	0.75	0.1456(2)	0.0074(4)
O(6)	0.0674(2)	0.75	0.4069(2)	0.0090(4)
O(7)	0.5152(3)	0.75	0.1799(2)	0.0114(4)
O(8)	0.5243(3)	0.25	0.3080(2)	0.0134(5)
O(9)	0.6290(3)	0.25	0.0991(2)	0.0146(5)
O(10)	0.0827(2)	0.25	0.4290(2)	0.0081(4)
H(1)	0.0739*	0.25	0.333*	0.072(17)

Note: Al[M(1)]=100%; Al[M(2)]=100%; Al[M(3)]=29.4(4)% and Fe[M(3)]=70.6(4)%. *Not refined.

Table 2b. Refined fractional atomic coordinates and equivalent isotropic temperature factors ($\mathring{A}^2$), with standard deviations in parentheses, based on the diffraction data collected at 100 K. U_{eq} is defined as one third of the trace of the orthogonalised U_{ij} tensor.

Site	x/a	y/b	z/c	U_{eq}
Ca(1)	0.75776(8)	0.75	0.15185(7)	0.00678(13)
Ca(2)	0.60651(9)	0.75	0.42509(7)	0.00792(13)
Si(1)	0.34012(11)	0.75	0.04823(9)	0.00542(18)
Si(2)	0.68391(12)	0.25	0.27519(9)	0.00572(18)
Si(3)	0.18396(11)	0.75	0.31839(9)	0.00526(18)
M(1)	0	0	0	0.00429(18)
M(2)	0	0	0.5	0.00557(19)
M(3)	0.29333(7)	0.25	0.22385(6)	0.00476(16)
O(1)	0.23384(18)	-0.0055(3)	0.04140(15)	0.0067(3)
O(2)	0.3035(2)	-0.0177(3)	0.35483(16)	0.0071(3)
O(3)	0.7945(2)	0.0133(3)	0.33978(16)	0.0077(3)
O(4)	0.0524(3)	0.25	0.1300(2)	0.0067(4)
O(5)	0.0409(3)	0.75	0.1449(2)	0.0061(4)
O(6)	0.0669(3)	0.75	0.4063(2)	0.0070(4)
O(7)	0.5154(3)	0.75	0.1812(2)	0.0080(4)
O(8)	0.5240(3)	0.25	0.3076(2)	0.0114(5)
O(9)	0.6285(3)	0.25	0.0988(2)	0.0110(5)
O(10)	0.0825(3)	0.25	0.4280(2)	0.0064(4)
H(1)	0.0639*	0.25	0.3294*	0.034(13)

Note: Al[M(1)]=100%; Al[M(2)]=100%; Al[M(3)]= 30.5(4)% and Fe[M(3)]= 69.6(4)%. *Not refined.

Table 3a. (Deposited) Refined displacement parameters (Å^2) in the expression: $-2\pi^2[(ha^*)^2U_{11} + ... + 2hka^*b^*U_{12} + ... + 2klb^*c^*U_{23}]$, based on the data collected at 295 K.

Site	U_{11}	U_{22}	U_{33}	U_{12}	U_{13}	U_{23}
Ca(1)	0.0143(3)	0.0111(3)	0.0099(3)	0	0.0078(2)	0
Ca(2)	0.0127(3)	0.0194(4)	0.0080(3)	0	0.0037(2)	0
Si(1)	0.0067(4)	0.0073(4)	0.0063(3)	0	0.0028(3)	0
Si(2)	0.0081(4)	0.0064(4)	0.0074(3)	0	0.0035(3)	0
Si(3)	0.0067(4)	0.0081(4)	0.0054(3)	0	0.0027(3)	0
M(1)	0.0066(4)	0.0060(4)	0.0055(4)	0.0000(3)	0.0020(3)	0.0000(3)
M(2)	0.0074(4)	0.0059(4)	0.0073(4)	0.0001(3)	0.0034(3)	0.0002(3)
M(3)	0.0064(3)	0.0087(3)	0.0063(2)	0	0.00232(18)	0
O(1)	0.0074(7)	0.0066(7)	0.0114(6)	0.0003(6)	0.0032(5)	0.0007(5)
O(2)	0.0102(7)	0.0112(7)	0.0083(6)	-0.0015(6)	0.0043(5)	0.0003(5)
O(3)	0.0089(7)	0.0086(7)	0.0112(6)	-0.0006(6)	0.0003(5)	-0.0009(5)
O(4)	0.0084(10)	0.0082(10)	0.0061(9)	0	0.0026(8)	0
O(5)	0.0073(10)	0.0077(10)	0.0061(8)	0	0.0017(7)	0
O(6)	0.0105(11)	0.0081(10)	0.0104(9)	0	0.0064(8)	0
O(7)	0.0112(11)	0.0133(11)	0.0089(9)	0	0.0034(8)	0
O(8)	0.0131(11)	0.0159(12)	0.0157(10)	0	0.0103(9)	0
O(9)	0.0155(12)	0.0214(13)	0.0084(9)	0	0.0064(9)	0
O(10)	0.0102(10)	0.0070(10)	0.0088(9)	0	0.0058(8)	0

Table 3b. (Deposited) Refined displacement parameters (Å^2) in the expression: $-2\pi^2[(ha^*)^2U_{11} + ... + 2hka^*b^*U_{12} + ... + 2klb^*c^*U_{23}]$, based on the data collected at 100 K.

Site	U_{11}	U_{22}	U_{33}	U_{12}	U_{13}	U_{23}
Ca(1)	0.0080(3)	0.0073(3)	0.0062(3)	0	0.0042(2)	0
Ca(2)	0.0078(3)	0.0109(3)	0.0047(3)	0	0.0024(2)	0
Si(1)	0.0056(4)	0.0066(4)	0.0041	0	0.0022(3)	0
Si(2)	0.0066(4)	0.0053(4)	0.0048(4)	0	0.0021(3)	0
Si(3)	0.0044(4)	0.0071(4)	0.0045(4)	0	0.0021(3)	0
M(1)	0.0049(4)	0.0042(5)	0.0039(4)	-0.0006(4)	0.0021(3)	-0.0006(3)
M(2)	0.0057(4)	0.0058(5)	0.0051(4)	0.0003(4)	0.0022(4)	-0.0002(4)
M(3)	0.0050(3)	0.0058(3)	0.0034(3)	0	0.0018(2)	0
O(1)	0.0063(7)	0.0061(7)	0.0080(7)	0.0001(6)	0.0033(6)	0.0006(6)
O(2)	0.0084(8)	0.0081(8)	0.0061(7)	-0.0021(6)	0.0040(6)	-0.0014(6)
O(3)	0.0070(7)	0.0068(8)	0.0074(7)	-0.0009(6)	0.0013(6)	-0.0011(6)
O(4)	0.0069(11)	0.0063(11)	0.0064(10)	0	0.0023(9)	0
O(5)	0.0055(11)	0.0074(11)	0.0047(9)	0	0.0016(8)	0
O(6)	0.0082(11)	0.0077(11)	0.0054(9)	0	0.0032(8)	0
O(7)	0.0073(11)	0.0079(11)	0.0068(10)	0	0.0012(9)	0
O(8)	0.0144(13)	0.0110(12)	0.0128(11)	0	0.0098(10)	0
O(9)	0.0123(13)	0.0153(12)	0.0071(10)	0	0.0056(9)	0
O(10)	0.0081(11)	0.0064(11)	0.0070(10)	0	0.0055(8)	0

Table 4a. Principal mean-square atomic displacements (U1, U2 and U3, Å^2) and root-mean-square components (R1, R2 and R3, Å) based on the structural refinement at 295 K.

Site	U1	U2	U3	R1	R2	R3	R1/R3
Ca(1)	0.0148(3)	0.0111(3)	0.0067(5)	0.122(1)	0.105(1)	0.082(3)	1.486
Ca(2)	0.0194(4)	0.0134(4)	0.0080(3)	0.139(1)	0.116(2)	0.089(2)	1.557
Si(1)	0.0073(4)	0.0067(5)	0.0063(4)	0.085(2)	0.082(3)	0.079(2)	1.076
Si(2)	0.0081(4)	0.0072(5)	0.0064(4)	0.090(2)	0.085(3)	0.080(2)	1.125
Si(3)	0.0081(4)	0.0068(5)	0.0054(5)	0.090(2)	0.082(3)	0.073(3)	1.225
M(1)	0.0073(7)	0.0060(4)	0.0054(3)	0.085(4)	0.077(3)	0.073(2)	1.163
M(2)	0.0076(3)	0.0069(7)	0.0059(4)	0.087(2)	0.083(4)	0.077(2)	1.135
M(3)	0.0087(3)	0.0070(5)	0.0061(2)	0.093(2)	0.084(3)	0.078(2)	1.194
O(1)	0.0123(10)	0.0075(6)	0.0065(7)	0.111(4)	0.087(3)	0.081(4)	1.376
O(2)	0.0125(8)	0.0093(6)	0.0075(11)	0.112(4)	0.096(3)	0.087(6)	1.291
O(3)	0.0173(13)	0.0090(7)	0.0067(6)	0.132(5)	0.095(4)	0.082(4)	1.607
O(4)	0.0089(15)	0.0082(10)	0.0061(9)	0.094(8)	0.091(5)	0.078(6)	1.208
O(5)	0.0089(16)	0.0077(10)	0.0058(7)	0.094(8)	0.088(6)	0.076(4)	1.239
O(6)	0.0118(7)	0.0081(10)	0.0070(19)	0.109(3)	0.090(6)	0.084(11)	1.298
O(7)	0.0133(11)	0.0123(18)	0.0088(8)	0.115(5)	0.111(8)	0.094(4)	1.229
O(8)	0.0174(8)	0.0159(12)	0.0069(20)	0.132(3)	0.126(5)	0.083(12)	1.588
O(9)	0.0214(13)	0.0155(12)	0.0070(14)	0.146(4)	0.124(5)	0.084(8)	1.748
O(10)	0.0108(8)	0.0070(10)	0.0064(17)	0.104(4)	0.084(6)	0.080(11)	1.299

Table 4b. Principal mean-square atomic displacements (U1, U2 and U3, Å^2) and root-mean-square components (R1, R2 and R3, Å) based on the structural refinement at 100 K.

Site	U1	U2	U3	R1	R2	R3	R1/R3
Ca(1)	0.0083(2)	0.0073(3)	0.0048(5)	0.091(1)	0.085(2)	0.069(4)	1.315
Ca(2)	0.0109(3)	0.0082(4)	0.0046(3)	0.104(1)	0.091(2)	0.068(2)	1.539
Si(1)	0.0066(4)	0.0056(5)	0.0040(5)	0.081(2)	0.075(3)	0.063(4)	1.284
Si(2)	0.0070(6)	0.0053(4)	0.0048(4)	0.084(4)	0.073(3)	0.069(3)	1.208
Si(3)	0.0071(4)	0.0046(3)	0.0040(8)	0.084(2)	0.068(2)	0.063(6)	1.332
M(1)	0.0053(4)	0.0042(6)	0.0034(5)	0.073(3)	0.065(5)	0.058(4)	1.248
M(2)	0.0062(6)	0.0055(4)	0.0050(5)	0.079(4)	0.074(3)	0.071(4)	1.114
M(3)	0.0058(3)	0.0051(4)	0.0033(3)	0.076(2)	0.071(3)	0.057(3)	1.326
O(1)	0.0081(7)	0.0061(9)	0.0058(10)	0.089(4)	0.078(6)	0.076(7)	1.174
O(2)	0.0104(7)	0.0061(9)	0.0049(10)	0.102(3)	0.078(6)	0.070(8)	1.457
O(3)	0.0103(14)	0.0076(7)	0.0051(6)	0.101(7)	0.087(4)	0.071(4)	1.421
O(4)	0.0076(19)	0.0063(11)	0.0062(8)	0.087(11)	0.079(7)	0.079(5)	1.107
O(5)	0.0074(11)	0.0062(17)	0.0046(8)	0.086(6)	0.079(11)	0.068(6)	1.268
O(6)	0.0082(13)	0.0077(11)	0.0050(13)	0.090(7)	0.088(6)	0.071(10)	1.281
O(7)	0.0102(20)	0.0079(11)	0.0058(7)	0.101(10)	0.089(6)	0.076(4)	1.326
O(8)	0.0165(10)	0.0110(12)	0.0066(22)	0.128(4)	0.105(6)	0.081(13)	1.581
O(9)	0.0153(12)	0.0123(12)	0.0055(16)	0.124(5)	0.111(5)	0.074(11)	1.668
O(10)	0.0092(8)	0.0064(11)	0.0035(19)	0.096(4)	0.080(7)	0.059(16)	1.621

Table 5. Relevant bond distances (Å) and angles (°) based on the diffraction data collected at 295 and 100 K.

	298 K		100 K	
Ca1-O1 x 2	2.454(1)	2.462*	2.459(1)	2.462*
Ca1-O3 x 2	2.326(2)	2.335*	2.326(2)	2.331*
Ca1-O5	2.550(2)	2.561*	2.548(2)	2.554*
Ca1-O6	2.860(2)	2.873*	2.856(2)	2.862*
Ca1-O7	2.294(2)	2.303*	2.299(2)	2.303*
Ca1-O9 x 2	2.995(1)	3.303*	3.002(1)	3.007*
<Ca1-O>	2.584		2.586	
Ca2-O2 x 2	2.531(2)	2.542*	2.525(2)	2.530*
Ca2-O2` x 2	2.786(2)	2.799*	2.799(2)	2.804*
Ca2-O3 x 2	2.649(2)	2.659*	2.642(2)	2.647*
Ca2-O7	2.255(2)	2.266*	2.252(2)	2.256*
Ca2-O8	3.013(1)	3.020*	3.023(1)	3.030*
Ca2-O10	2.525(2)	2.536*	2.519(2)	2.525*
<Ca2-O>	2.636		2.636	
Si1-O1 x 2	1.649(2)		1.655(2)	
Si1-O7	1.564(2)		1.566(2)	
Si1-O9	1.629(2)		1.631(2)	
<Si1-O>	1.623		1.627	
M.P.Q.E	1.0036		1.0035	
AV	10.73		10.20	
V (Å^3)	2.183(7)		2.198(7)	
Si2-O3 x 2	1.618(2)		1.619(2)	
Si2-O8	1.592(2)		1.591(2)	
Si2-O9	1.635(2)		1.641(2)	
<Si2-O>	1.616		1.618	
M.P.Q.E	1.0010		1.0011	
AV	4.2810		4.2920	
V (Å^3)	2.162(7)		2.169(7)	
Si3-O2 x 2	1.622(2)		1.625(2)	
Si3-O6	1.638(2)		1.635(2)	
Si3-O5	1.667(2)		1.674(2)	
<Si3-O>	1.637		1.640	
M.P.Q.E	1.0048		1.0049	
AV	19.0980		19.28	
V (Å^3)	2.236		2.248	
M1-O1 x 2	1.939(1)		1.937(1)	
M1-O4 x 2	1.841(1)		1.848(1)	
M1-O5 x 2	1.957(1)		1.955(1)	
<M1-O>	1.913		1.913	
M.P.Q.E	1.0064		1.0061	
AV	17.3110		17.3960	
V (Å^3)	9.247(14)		9.260(14)	
M2-O3 x 2	1.853(1)		1.857(1)	
M2-O6 x 2	1.927(1)		1.929(1)	
M2-O10 x 2	1.868(1)		1.874(1)	
<M2-O>	1.883		1.887	
M.P.Q.E	1.0044		1.0043	
AV	13.8150		13.5120	
V (Å^3)	8.846(15)		8.904(15)	
M3-O1 x 2	2.228(1)		2.223(1)	
M3-O2 x 2	1.984(2)		1.986(2)	
M3-O4	1.931(2)		1.937(2)	
M3-O8	1.855(2)		1.854(2)	
<M3-O>	2.035		2.035	
M.P.Q.E	1.0291		1.0283	
AV	76.0050		74.4260	
V (Å^3)	10.848(20)		10.851(20)	
O(10) - H(1)	0.925(2)		0.942(2)	
O(10)···O(4)	2.937(3)		2.920(3)	
H(1)···O(4)	2.016(2)		1.983(2)	
O(10) – H(1)···O4	173.9(10)		173.6(11)	
O(10)···O(2)	2.823(3)		2.817(3)	
H(1)···O(2)	2.472(2)		2.531(2)	
O(10) – H(1)···O2	102.0(10)		98.0(10)	

	298 K	100 K
O7-Si1-O9	106.57(12)	106.98(13)
O9-Si1-O1	106.32(7)	106.24(7)
O1-Si1-O1	112.87(11)	112.10(7)
O8-Si2-O3	110.95(7)	110.98(8)
O3-Si2-O3	110.37(11)	110.81(12)
O8-Si2-O9	110.83(12)	110.33(13)
O3-Si2-O9	106.79(7)	106.79(8)
O2-Si3-O2	106.91(11)	107.19(12)
O2-Si3-O6	112.49(7)	112.50(7)
O2-Si3-O5	111.69(7)	111.61(7)
O6-Si3-O5	101.67(11)	101.49(12)
O4-M1-O1`	86.34(8)	86.42(8)
O4-M1-O1	93.66(8)	93.58(6)
O4-M1-O5`	95.82(6)	95.88(6)
O4-M1-O5	84.18(6)	84.12(6)
O1-M1-O5	89.42(7)	89.33(8)
O1-M1-O5`	90.58(7)	90.67(8)
O3-M2-O10	88.17(8)	88.23(8)
O3-M2-O10`	91.83(8)	91.77(8)
O3-M2-O6	90.26(7)	90.39(8)
O3-M2-O6`	89.74(7)	89.61(8)
O10-M2-O6`	95.88(6)	95.82(7)
O10-M2-O6	84.12(6)	84.18(7)
O8-M3-O4	177.65(9)	178.08(10)
O8- M3-O2	88.2(6)	88.18(6)
O4-M3-O2	93.33(6)	93.07(6)
O2-M3-O2	98.88(8)	98.75(9)
O8-M3-O1	101.68(6)	101.80(6)
O4-M3-O1	76.56(6)	76.76(6)
O2-M3-O1	167.14(6)	167.24(6)
O2-M3-O1	89.73(5)	89.59(6)
O8-M3-O1	101.68(6)	101.80(7)
Si2-O9-Si1	155.45(8)	155.36(14)

* Bond distance corrected for "non-correlated motion" following Busing and Levy (1964). M..P.Q.E. is the "mean polyhedral quadratic elongation" and AV is the "angular variance" as defined by Robinson et al. (1971).

Table 6 (Deposited). Atomic positions, thermal displacement parameters, bond distances and angles and other geometrical parameters of epidotes at different temperatures.

Table 7. Results of FTIR spectral fitting for epidote over the wavenumber range 4,000-2,800 cm^{-1}. Spectra were fitted following thickness correction and after subtraction of a linear background over the range 4,000-2,500 cm^{-1} using Lorentzian peak profiles following the procedure outlined in the text and after Bromiley et al. (2010). Assignment of fitted peaks to OH bands, and proposed H incorporation mechanisms, as discussed in the text, are given.

Spectrum	Peak	Position	Position esd	Area	Area esd	Width	Width esd	Suggested OH band assignment
E//a	A1	3256.7	3.5	84.2	8.2	144.5	11.6	Band 5: OH vibration coupled with lattice vibration
	A2	3371.0	2.6	40.2	9.7	78.4	13.2	Unresolved doublet corresponding to Bands 3+4?
	A3	3464.2	6.8	60.7	12.1	142.9	20.2	Band 1: OH vibration coupled with lattice vibration
E//b	B1	3254.9	1.9	29.3	2.2	82.9	6.6	Band 5: OH vibration coupled with lattice vibration
	B2	3352.3	1.7	28.7	6.2	50.6	6.2	Band 3: $^{[M1,2]}Al_2$-O(10)-H(1)$\cdots$O(4)-$^{[M1,2]}Al_2^{[M3]}Al$
	B3	3399.8	0.8	117.5	10.5	68.3	4.2	Band 2: O(10)–H(1)$\cdots$O(2)?
	B4	3464.8	1.4	49.1	4.9	67.2	4.2	Band 1: OH vibration coupled with lattice vibration
E//c	C1	3257.3	0.3	896.2	9.8	97.1	1.0	Band 5: OH vibration coupled with lattice vibration
	C2	3352.1	0.1	1611.9	31.3	42.0	0.4	Band 3: $^{[M1,2]}Al_2$-O(10)-H(1)$\cdots$O(4)-$^{[M1,2]}Al_2^{[M3]}Al$
	C3	3385.9	0.3	2385.1	45.1	68.4	0.7	Band 4: $^{[M1,2]}Al_2$-O(10)-H(1)$\cdots$O(4)-$^{[M1,2]}Al_2^{[M3]}Fe^{3+}$
	C4	3469.5	0.3	541.5	11.9	65.8	1.1	Band 1: OH vibration coupled with lattice vibration

Fig. 1. Two views of the crystal structure of epidote, based on the atomic coordinates refined in this study at 295. The H-bonding scheme is shown [*i.e.* O(10)–H(1)···O(4); O(10)–H(1)···O(2)]. Thermal ellipsoid probability factor: 99%.
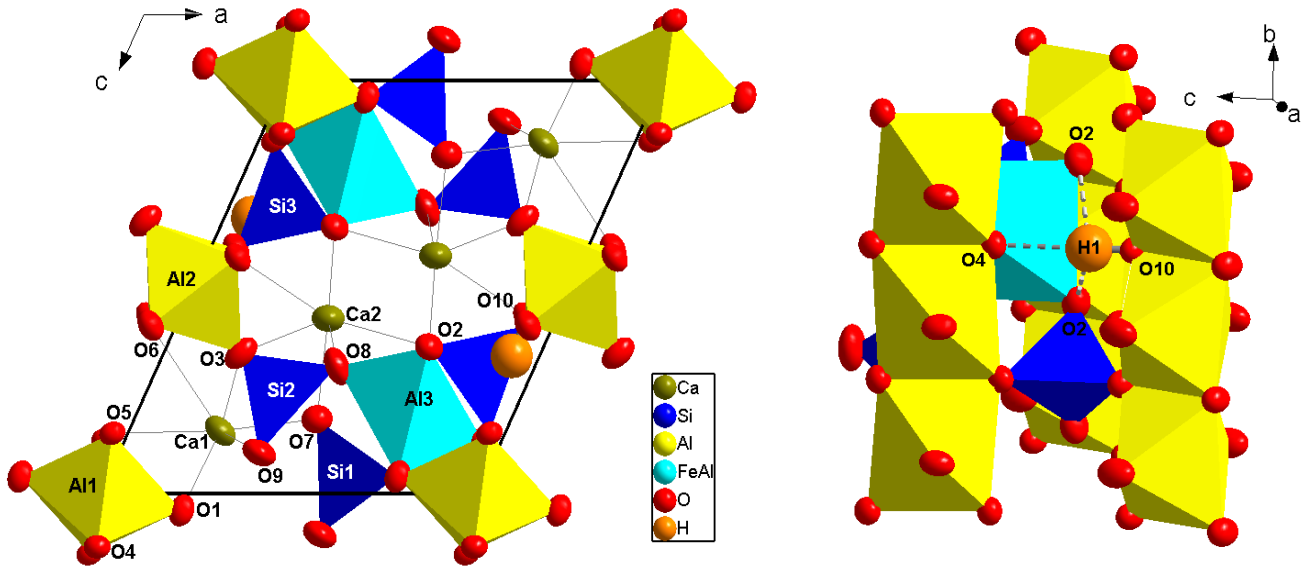
Fig. 2. Thickness corrected and background subtracted polarised FT-IR spectra from single crystal epidote showing absorption due to O-H stretching. Spectra obtained using radiation polarized with respect to the principle crystallographic axes: blue E//[001], black E//[010], red E//[100]. Insert shows vertically exaggerated E//[010] spectra with interference from anomalous H_2O and CO_2 species in the microscope optics removed for clarity. Ticks refer to the positions of bands determined from spectral deconvolution, as outlined in the text, and are labeled in accordance with Table 7.
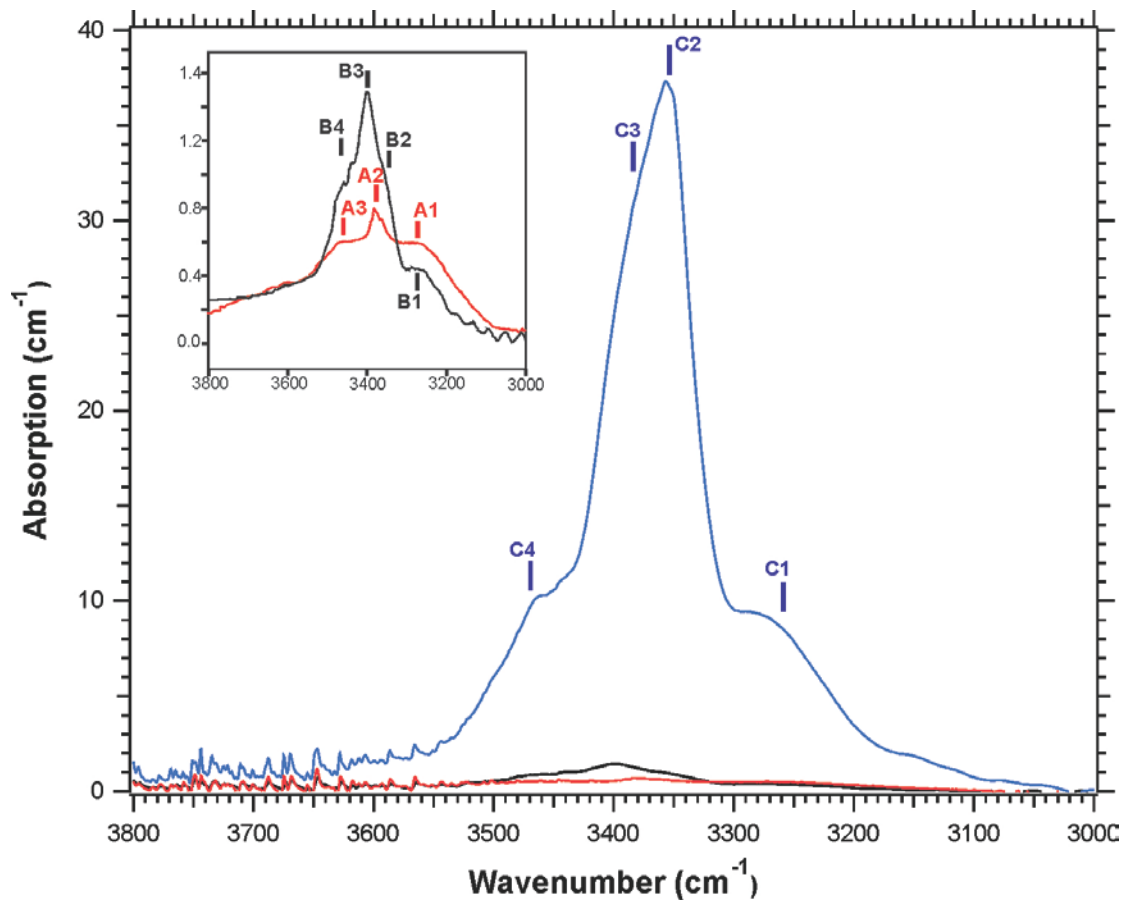
Fig. 3. Polarized FT-IR spectrum from epidote for E//[001] (as in Fig. 2) showing the results of band deconvolution. The spectrum was fitted using 4 Lorentzian peaks after background correction. Open red circles are actual IR data, the thick blue line is the fit to the data obtained using the four peaks shown with thin black lines. The residual between actual and fitted spectra is shown offset vertically by green diamonds.
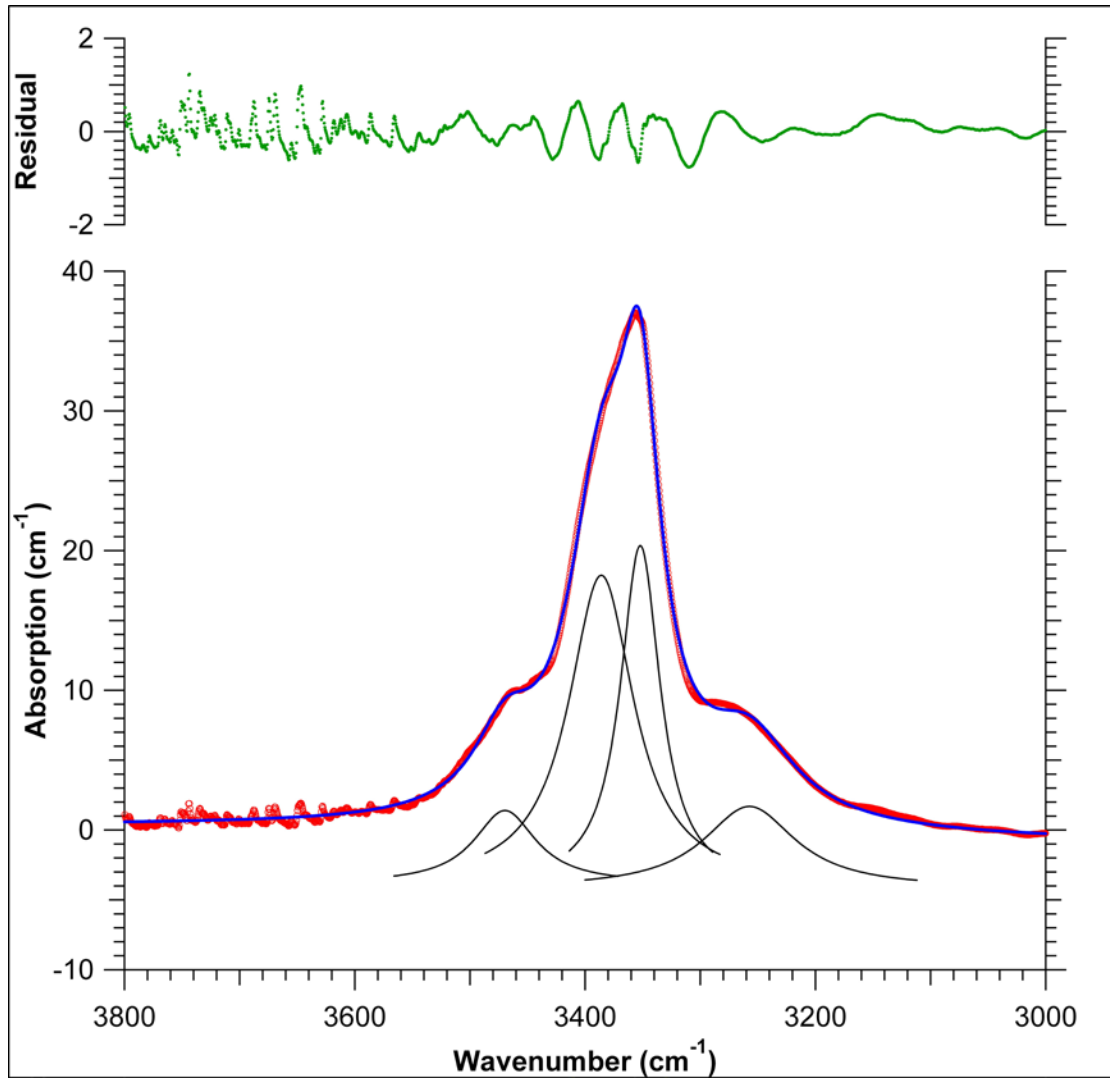
Fig. 4. Evolution of the unit-cell constants of epidote with *T*. Data points at *T*>298 K after Gatta et al. (2001); data points at *T*<298 K (collected increasing *T*) from this study. The solid lines represent the thermal equations reported by Gatta et al. (2001) (see text).
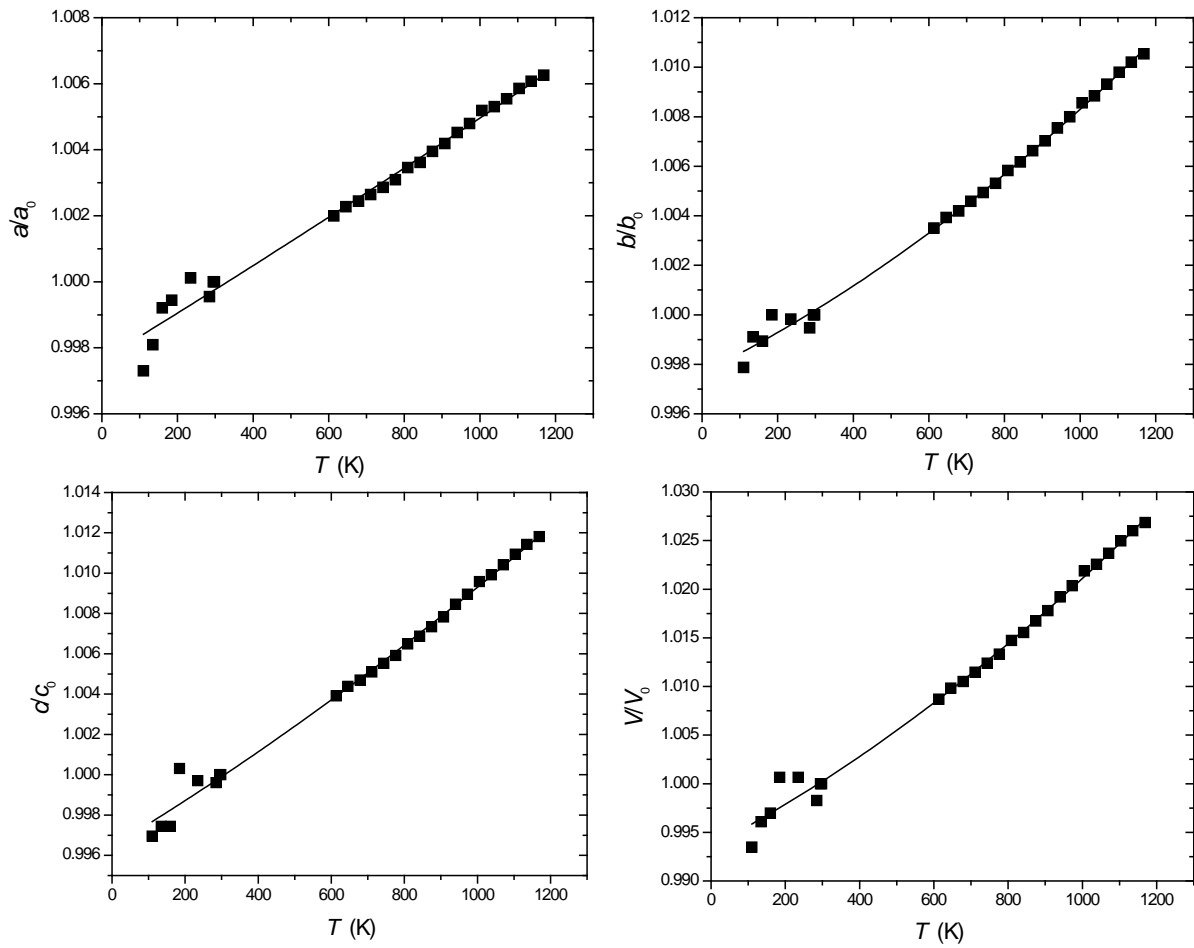
Fig. 5. Vibrational regime of the atomic sites belonging to the coordination shell of the Ca(1) and Ca(2) sites at 295 K (*left side*) and 100 K (*right side*). Thermal ellipsoid probability factor: 99%.
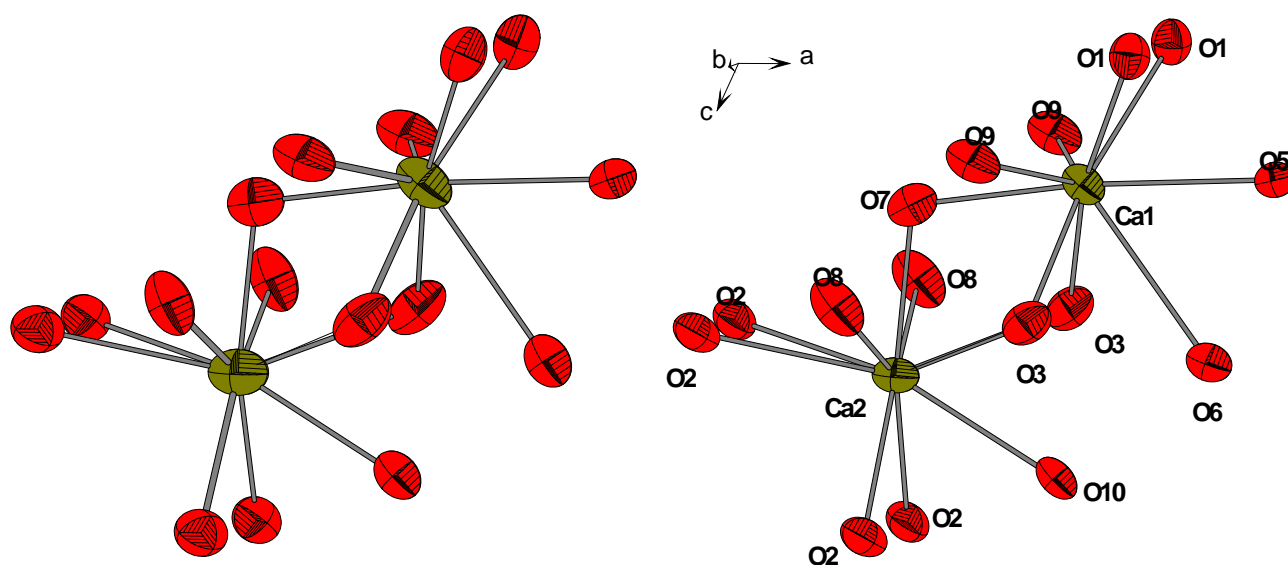
Fig. 6. Evolution of the U_{eq} and of the root-mean-square components (R1, R2 and R3) of the Ca(1) and Ca(2) sites with T.